Galactic Superwinds

by **Sergiy Silich**
Instituto National de Astrofisica Optica y Electronica, Mexico

1 Motivation

Massive starbursts are among the intrinsic characteristics of the evolution of galaxies. They are found both at high and intermediate redshifts (Dawson et al., 2002; Ajiki et al., 2002; Pettini et al., 1998) as well as in galaxies in the Local universe (Marlowe et al., 1995, Cairos et al. 2001).

The large kinetic energy deposited by the central star cluster is well known to drastically affect the surrounding interstellar medium, generating giant superbubbles seeing in radio, optical and X-ray emmision. The associated large-scale biconical gaseous outflows are oftern considered to be the tracers of supergalactic winds which transport energy, momentum and SNe ejected metals into the intergalactic medium. However to develop a true SGW the ISM has to be punched out by the shock wave and a free path into the intergalactic medium has to be opened. This is highly dependent both on the host galaxy and starburst properties.

HST imaging studies of extragalactic star-forming systems led to discovery of a new class of compact and high luminouse star clusters known as super star clusters or young massive clusters. Superwinds driven by these super star clusters seem to be very different from what was usually considered to be a supergalactic winds.

Collaborators: Guillermo Tenorio-Tagle, Casiana Muñoz-Tuñón, Roberto Terlevich, Elena Terlevich, Francois Legrand, Daniel Kunth, Miguel Cerviño, Luz Marina Cairos, Gil de Paz A., Hagai Netzer

Reference to:

- Silich & Tenorio-Tagle, 2001, ApJ, 552, 91
- Silich, S.. Tenorio-Tagle, G. Terlevich,R., Terlevich, E. & Netzer, H., 2001, MNRAS, 324, 191
- Legrand, Tenorio-Tagle, Silich, Kunth & Cervino, 2001, ApJ, 560, 630
- Gil de Paz, A., Silich, S.A., Madore, B.F., Contreras, C.S., Zamorano, J. & Gallego, J., 2002, ApJ, 573, L101
- Silich, S.A., Tenorio-Tagle, G., Muñoz-Tuñon C. & Cairos L.M., 2002, AJ, 123, 2438
- Silich, S., Tenorio-Tagle G. & Muñoz-Tuñón, C., 2003, ApJ (submitted)
- Tenorio-Tagle G., Silich, S. & Muñoz-Tuñón, C., 2003, in RevMexAA Conf. Ser. "8th Tex-Mex Conference on Astrophysics" Edts. M. Reyes-Ruiz and E. Vázquez-Semadeni (submitted)

2 PLAN OF THE PRESENTATION

- **Superbubbles vs Superwinds**
  - Thick vs thin disc model
  - Comparison with a sample of star-forming galaxies
  - Individual objects
- **Superwinds driven by super star clusters**
  - SSC basic properties
  - Impact of cooling
  - X-ray and emission line properties
  - X-ray emission problems

3 Superbubbles vs Superwinds

The KEY QUESTION: WHAT IS THE MECHANICAL ENERGY INPUT RATE WHICH IS REQUIRED TO EJECT THE NEWLY PROCESSED METALS OR MOST OF THE ISM OUT OF THE HOST GALAXY?

3.1 Thin disk model

Mac Low & Ferrara(1999) have reexamined previous results taking into account the impact of the DM halo.

The model includes only two components: Dark matter (DM) and ISM.

The Interstellar medium mass and gas velocity dispersion have been taken as free parameters.

Problems: The interstellar gas velocity dispersion was taken to be small. Therefore in the horizontal direction equilibrium is supported by the centrifugal forces. The ISM is not in pressure balance with the intergalactic medium.

3.2 Equilibrium model

Two basic points have been revised:

- The rotational properties of the gaseous component
- The pressure balance between the interstellar and intergalactic media

The equilibrium model has three free parameters: the ISM mass M_{ISM}, the fraction of the radial component of gravity which is balanced by the pressure gradients (1 - ϵ) and the external intracluster medium pressure (P_{IGM}).

We derive the central gas density ρ_0 and gas velocity dispersion C_{ISM} from the condition that the galaxy is stable and that its ISM is in pressure balance with the intracluster medium at the galaxy outer boundary.

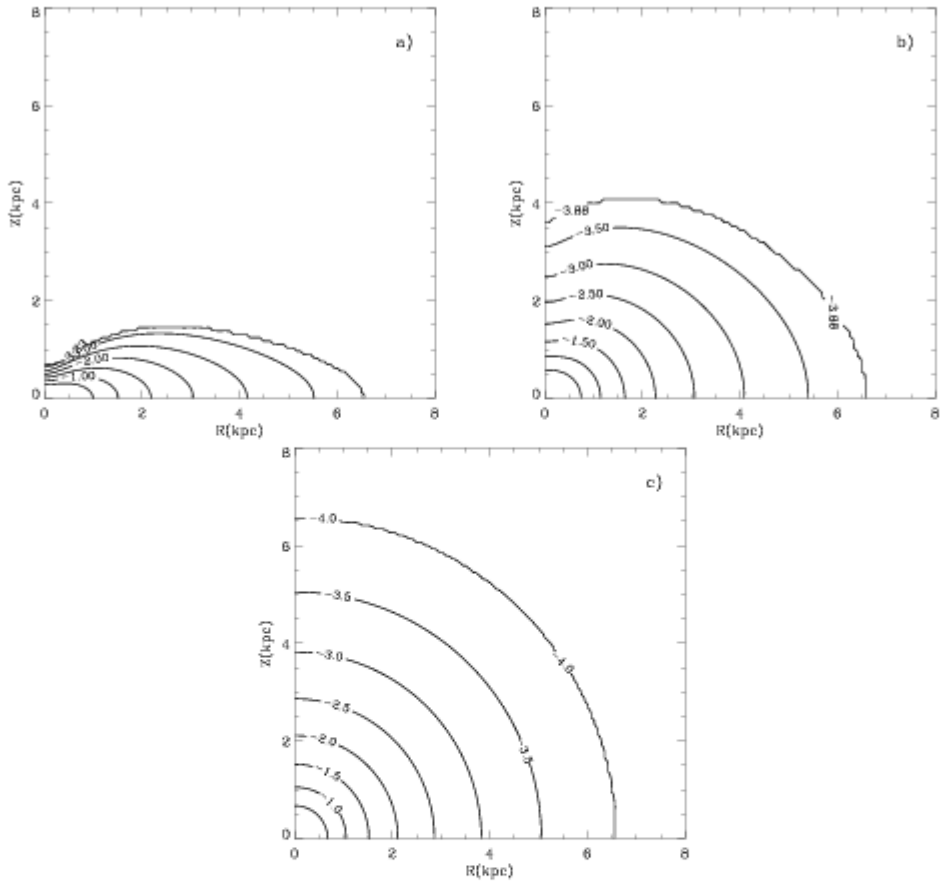


Figure 1: **The ISM gas distribution for $M_{ISM} = 10^8$ $M_\odot$ galaxy with different amount of rotation. Panels a), b) and c) represent the gas distribution for 19%, 75% and 100% of the radial component of gravity balanced by pressure gradients, respectively.**

3.3 Comparison with a sample of star-forming galaxies

Table 1: **Star-forming dwarf galaxies. Observational data**

Name	M(HI) (10^8 $M_\odot$)	ref	12+Log(O/H)	ref	$L(H_\alpha)$ erg s^{-1}	ref
(1)	(2)	(3)	(4)	(5)	(6)	(7)
Haro-3	5.4	1	8.37	7	7.14×10^{40}	9*
Mkn-49/1318	1.9	1	8.28	14	3.71×10^{40}	10*
NGC-2915	5.9	18	8.4	7	1.30×10^{39}	8
Haro-2	4.6	1	8.4	6	1.20×10^{41}	6*
II-Zw-70	3.4	1	8.07	6	2.23×10^{40}	6*
I-Zw-18	0.26	6	7.18	6	4.29×10^{39}	6*
Haro-14	3.2	1	8.4	13	9.03×10^{39}	9*
IC-10	13	3	8.29	3	2.70×10^{40}	11
GR-8	0.098	4	7.68	15	1.43×10^{38}	9*
DDO-167	0.14	2	7.66	16	7.08×10^{37}	11
DDO-53	0.54	2	7.62	16	6.30×10^{38}	11
WLM	0.56	2	7.74	16	7.40×10^{38}	11
IC-1613	0.49	2	7.86	16	5.25×10^{38}	11
Sex-A	0.79	2	7.49	16	1.40×10^{39}	11
Sex-B	0.44	2	7.56	16	4.07×10^{38}	11
NGC-6822	0.66	2	8.14	16	3.89×10^{39}	11
DDO-47	2.51	2	7.85	16	2.34×10^{38}	11
NGC-2366	7.94	2	7.96	16	1.58×10^{40}	11
NGC-1569	0.59	2	8.16	16	2.19×10^{41}	11
NGC-4214	10.96	2	8.34	16	3.71×10^{40}	11
NGC-4449	13.49	2	8.32	16	7.08×10^{40}	11
NGC-5253	2.04	2	8.27	17	1.97×10^{40}	12*

References: 1) Thuan & Martin, 1981 2) Karachentsev et al., 1999 3) Lequeux et al., 1979 4) Huchtmeier et al., 2000 5) Contini, 1996b 6) Mas-Hesse & Kunth, 1999 7) Papaderos et al., 1996 8) Marlowe et al., 1995 9) Gallagher, Hunter & Bushouse, 1989 10) Vilchez, 1995 11) Hunter, Hawley & Gallagher, 1993 12) Storchi-Bergmann, Kinney & Challis, 1995 13) Marlowe, Meurer & Heckman, 1999 14) Contini, 1996a 15) Moles et al., 1990 16) Skillman, Kennicutt & Hodge, 1989 17) Terlevich, Terlevich & Denicolo, 2001 18) Becker et al., 1988

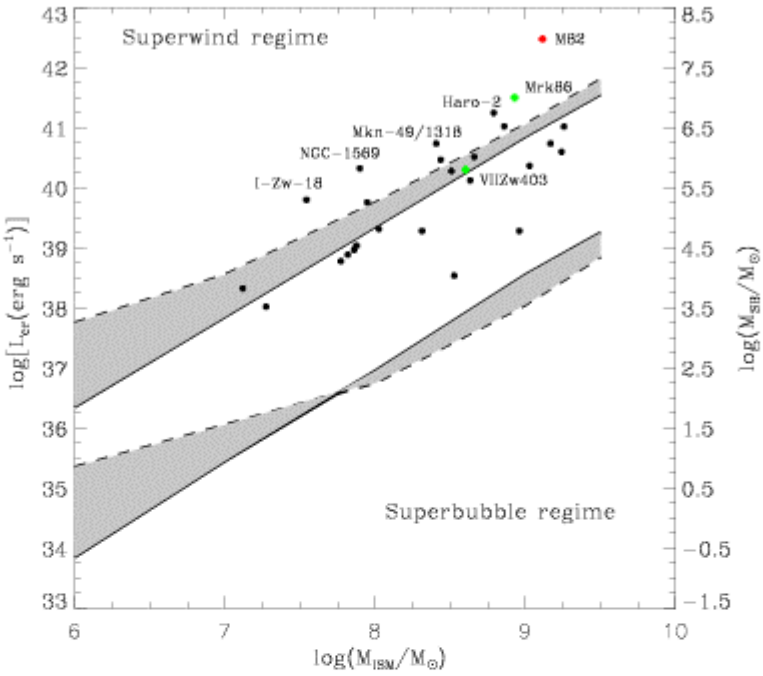


Figure 2: The comparison of the predicted critical mechanical luminosity with the sample of star forming galaxies.

3.4 Individual objects

VIIZW 403

Table 2: VII Zw403 observational properties

Parameter		Reference	Comments
Distance	4.5 Mpc	1	
The galaxy total mass	2×10^8 $M_\odot$	2	
The galaxy ISM mass	$(4-7) \times 10^7$ $M_\odot$	1, 2	from HI observations
The radius of the HI halo	$\sim$ 1.9 kpc		not well known, see text
The ISM gas velocity dispersion	$\sim$ 30 km s^{-1}	2	
The ISM gas metalicity	(0.05 - 0.06)$Z_\odot$	3	
The total H_α flux	$(195 \pm 4) \times 10^{-13}$ ergs cm^{-2} s^{-1}	our data	integrated out to the limiting isophote
The total H_α luminosity	1.8×10^{39} ergs s^{-1}	1	
	4.7×10^{40} ergs s^{-1}	our data	
H_α shell radii			
- Large	$\sim$ 250 pc	our data	around association 4
- Small	$\sim$ 80 pc	1	around association 1
Diffuse X-ray emission:	$(1.9-2.3) \times 10^{38}$ ergs s^{-1}	4, 5	ROSAT PSPC data
- Unresolved core	$\sim$ 85%		not confirmed by
- Extended diffuse emission	$\sim$ 15%		ROSAT HRI data
X-ray flux from the point source	9×10^{-13} ergs cm^{-2} s^{-1}	6	ROSAT HRI data

References: 1) Lynds et al., 1998 2) Thuan & Martin, 1981 3) Schulte-Ladbeck et al., 1999 4) Papaderos et al., 1994 5) Fourniol, 1997 6) Lira et al., 2000

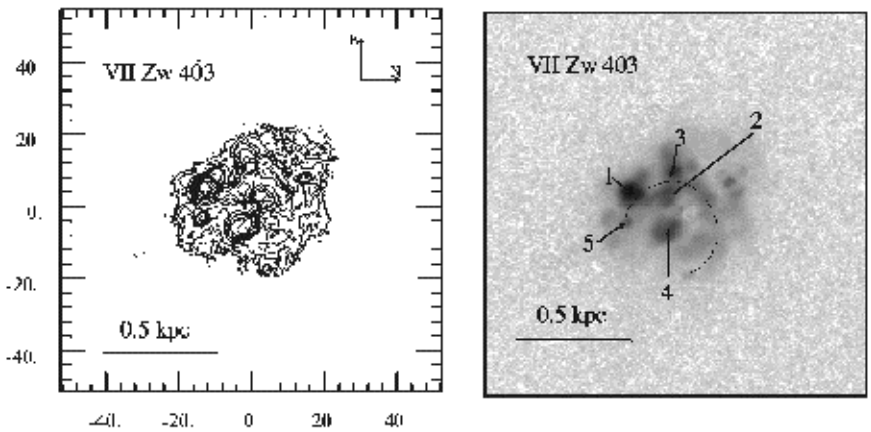


Figure 3: New narrow-band images of VII Zw403 centered on the H_α line and on the adjacent continuum (Figure 1) were taken in August 1997 at the 2.2-m telescope of the German–Spanish Astronomical Observatory at Calar Alto (Almería, Spain) with *Calar Alto Faint Object Spectrograph* and a 2048 × 2048 SiTe CCD chip. At the current epoch the main $H\alpha$ contribution comes from the few central knots with a strong star formation activity.

Mrk86

Table 3: **Mrk86 observational properties**

Parameter		Reference	Comments
Distance	6.9 Mpc	1	
Stellar disk mass	5×10^9 $M_\odot$		
DM mass	8×10^9 $M_\odot$		
The ISM mass	8.5×10^8 $M_\odot$	2	from HI observations
The ISM velocity dispersion	~ 35 km s^{-1}	our data	
The ISM metalicity	$(0.1 - 0.2)Z_\odot$		
SB mass	$\sim 10^7$ $M_\odot$	3	

References: 1) Sharina et al., 1999 2) Swaters, 1999 3) Gil de Paz et al. 2000

FIG. 1.— a) ^{12}CO(1-0) spectra averaged over the whole galaxy (*top panel*) and in the position of the galaxy center (*middle panel*) and of the Mrk 86-B bubble (*bottom panel*). In the upper panel the 21 cm HI-line profile obtained by Swaters (1999) is also shown (*dashed line*). The arrows drawn in the bottom panel mark the position of the approaching and receding parts of the Mrk 86-B bubble. b) The same for the ^{12}CO(2-1) emission.

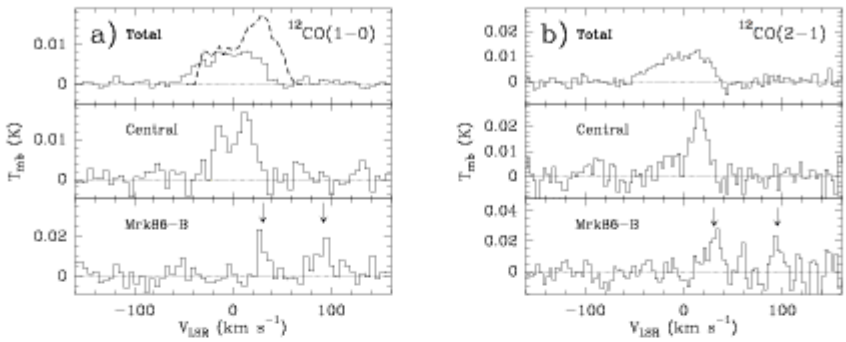
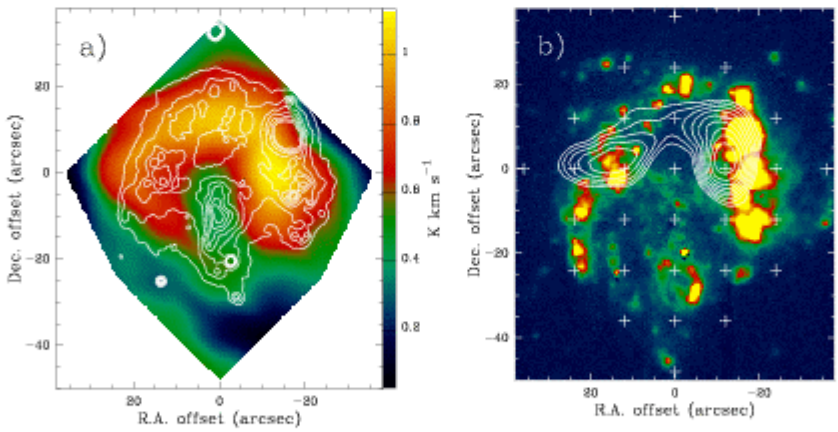


FIG. 2.— a) ^{12}CO(1-0) line emission map with the *R*-band contours overimposed. The horseshoe-like distribution of the gas is clearly seen around the position of the nuclear starburst. b) Hα image of Mrk 86 with the contours in ^{12}CO(2-1) line intensity ranging between 1.0 and 2.0 K km s^{-1} in steps of 0.1 K km s^{-1} overimposed.



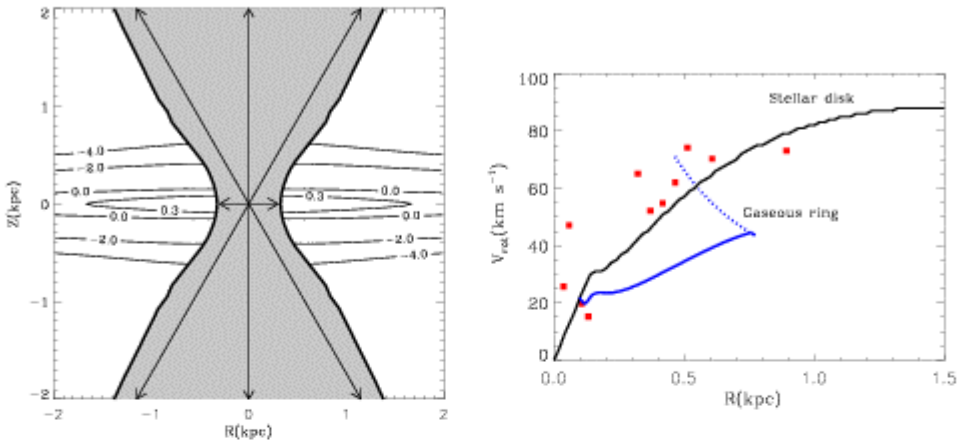


Figure 4: **Mrk86 superwind evolution. (a) The shape of the superwind cone after 5.5 Myr of energy deposition by the central star cluster; (b) Circular velocities of stellar disk and gaseous ring.**

4 Superwinds driven by super star clusters

4.1 SSC basic properties

Recent high-resolution HST observations revealed a number of young stellar clusters of extraordinary luminosity and compactness (Ho, 1997; Larsen, S.S. & Richtler, 2000). They are found in a variety of environments ranging from nearby dwarf galaxies to distant merging galaxies and circumnuclear rings.

Table 4: SSC basic properties

Masses	$10^5 - 10^6\,M_\odot$
Median half-light radii	≈ 3pc
Metallicities	from $1/50 Z_\odot$ to $\sim Z_\odot$

5 STEADY WIND SOLUTION

5.1 MAIN EQUATIONS. (Chevalier & Clegg, 1985)

$$\frac{1}{r^2}\frac{\mathrm{d}}{\mathrm{d}r}\left(\rho u r^2\right) = 0, \qquad \frac{1}{r^2}\frac{\mathrm{d}}{\mathrm{d}r}\left(\rho u r^2\right) = 0,$$

$$\rho u \frac{\mathrm{d}u}{\mathrm{d}r} = -\frac{\mathrm{d}P}{\mathrm{d}r}, \qquad \rho u \frac{\mathrm{d}u}{\mathrm{d}r} = -\frac{\mathrm{d}P}{\mathrm{d}r},$$

$$\frac{1}{r^2}\frac{\mathrm{d}}{\mathrm{d}r}\left[\rho u r^2\left(\frac{u^2}{2} + \frac{\gamma}{\gamma-1}\frac{P}{\rho}\right)\right] = 0, \qquad \frac{1}{r^2}\frac{\mathrm{d}}{\mathrm{d}r}\left[\rho u r^2\left(\frac{u^2}{2} + \frac{\gamma}{\gamma-1}\frac{P}{\rho}\right)\right] = -Q.$$

Three starburst parameters control this solution:

L_{tot} $\dot{M}_{tot}$ R_{SB}

Asymptotic solution

$\mathrm{V}_w \rightarrow \mathrm{V}_t \sim 1000$ km s^{-1}; $\rho_w \sim \mathrm{r}^{-2}$; $\mathrm{T}_w \sim \mathrm{r}^{-4/3}$

HOWEVER: IT HAS NEVER BEEN PROVED THAT COOLING IS INEFFECTIVE OUT OF THE STAR FORMING REGION

5.2 CHARACTERISTIC TIME SCALES

$$\tau_{cool}(r) = \frac{3kT}{n\Lambda}; \qquad \tau_{dyn}(r) = \int_{R_{SB}}^{r} \frac{\mathrm{d}r}{u(r)} \tag{1}$$

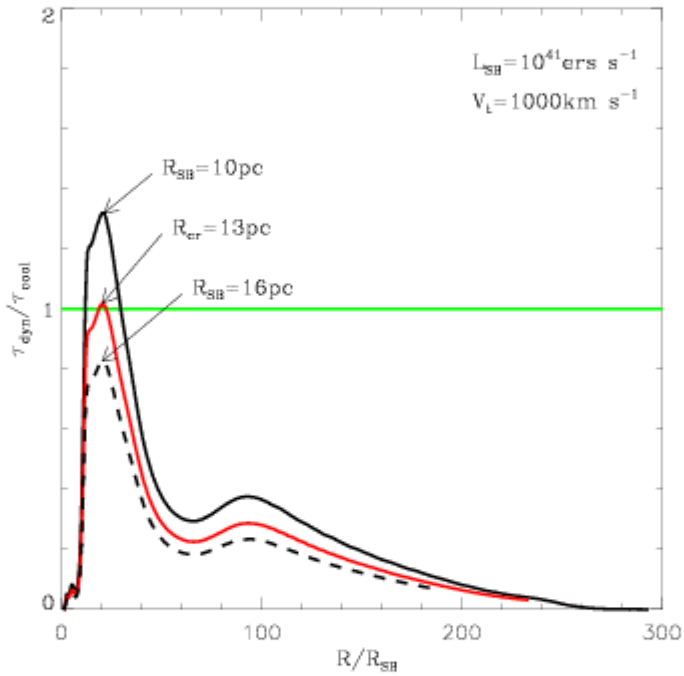


Figure 5: The intrinsic properties of superwinds. The ratio of characteristic time scales.

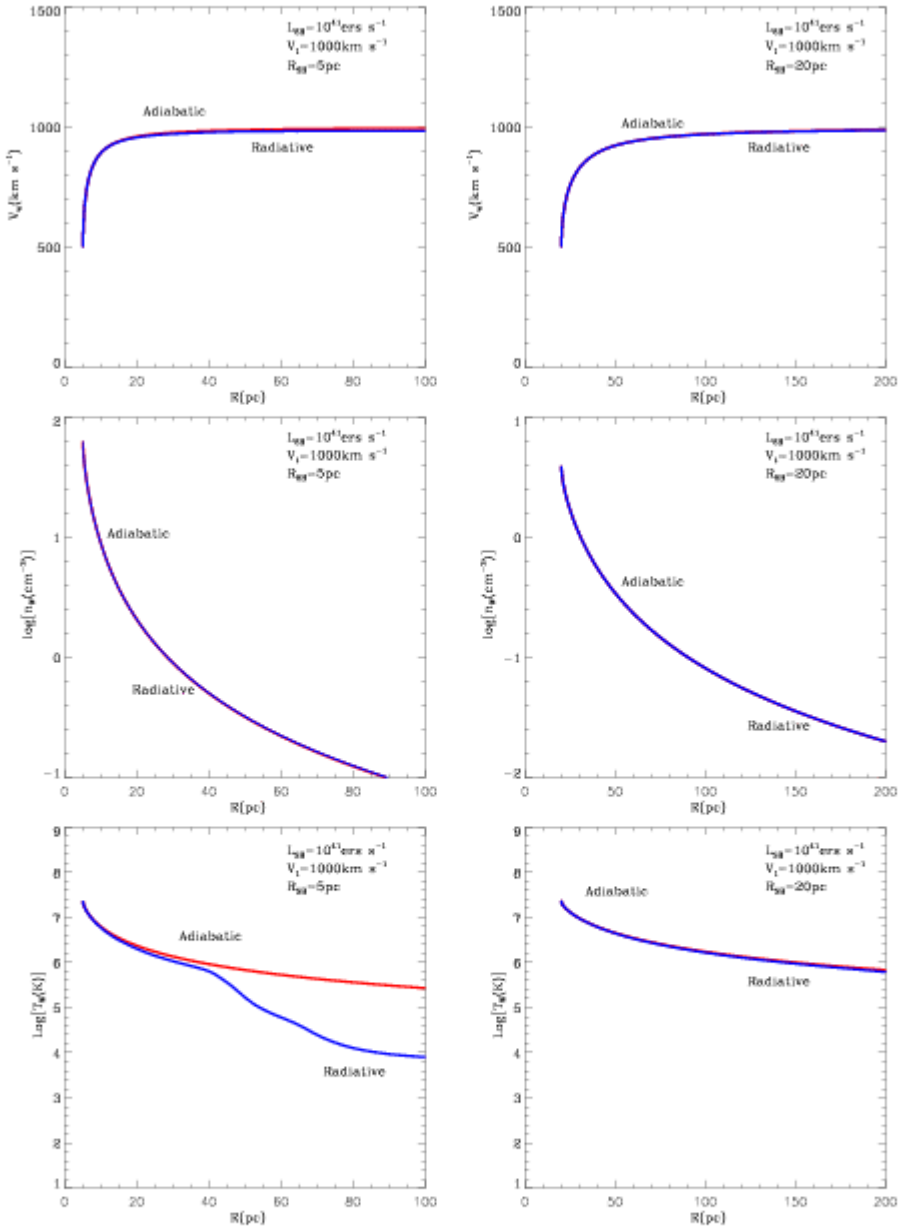


Figure 6: The intrinsic properties of superwinds. Velocity, density and temperature profiles.

5.3 CRITICAL STARBURST PARAMETERS

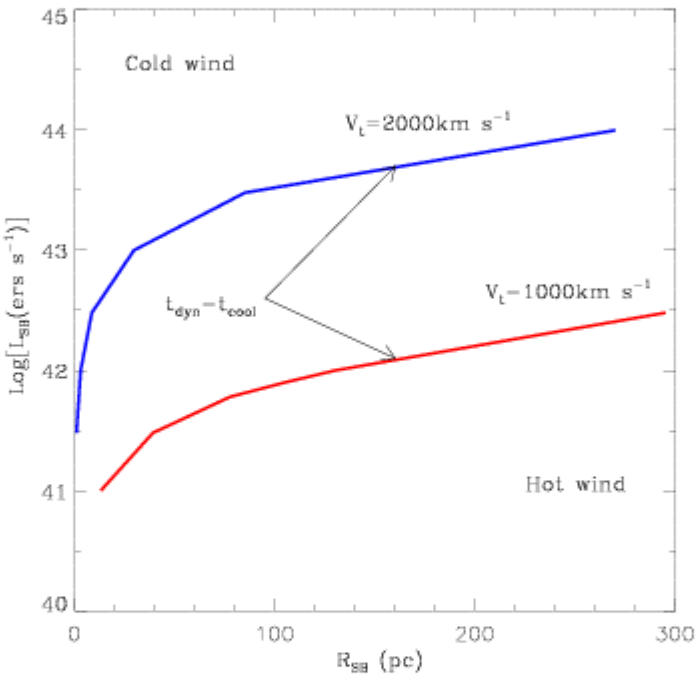


Figure 7: The initial parameter space for hot and cold superwind models

6 INTERNAL SUPERWIND STRUCTURE

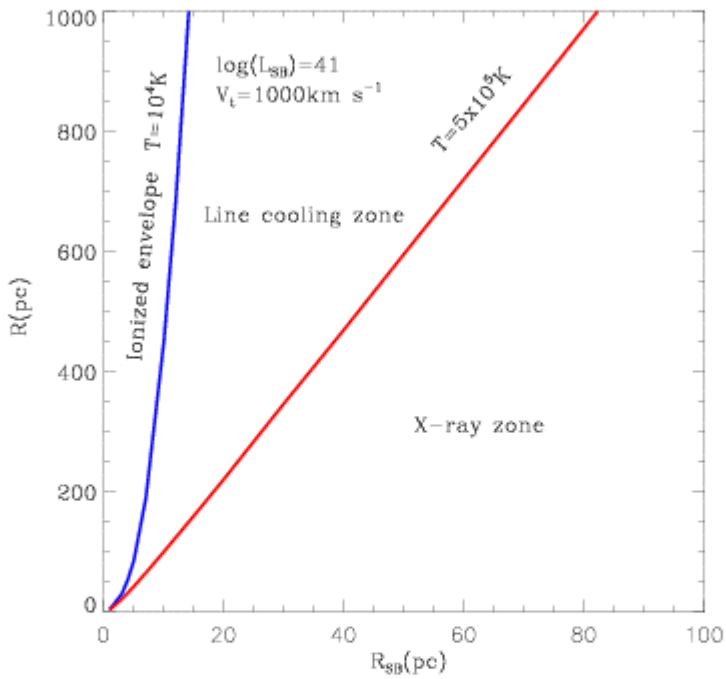


Figure 8: The internal structure of superwind

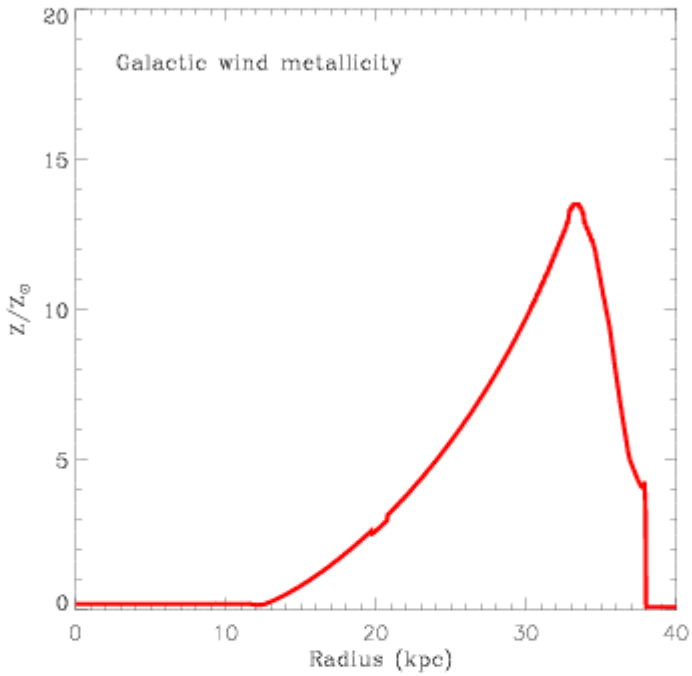


Figure 9: Galactic superwind metallicity

7 OBSERVATIONAL CONSEQUENCES

7.1 Broad line emission

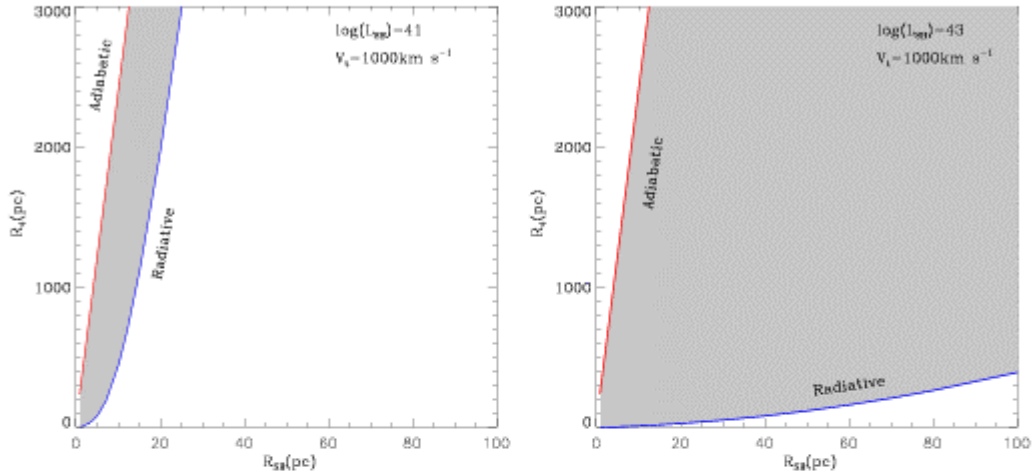


Figure 10: The inner radius (R_4) of the cold envelope with $T \leq 10^4$K as function of R_{SB}

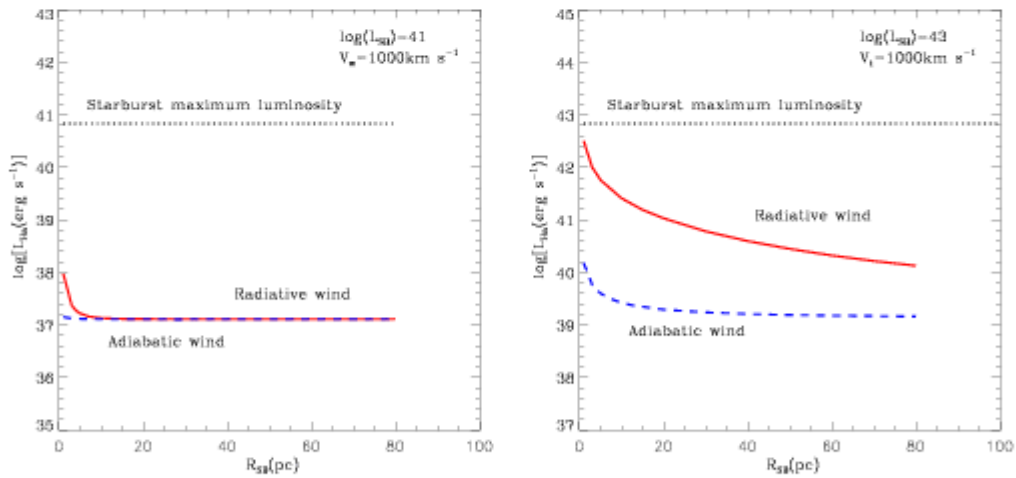


Figure 11: Superwind H_α luminosity as function of R_{SB}

7.2 X-ray emission

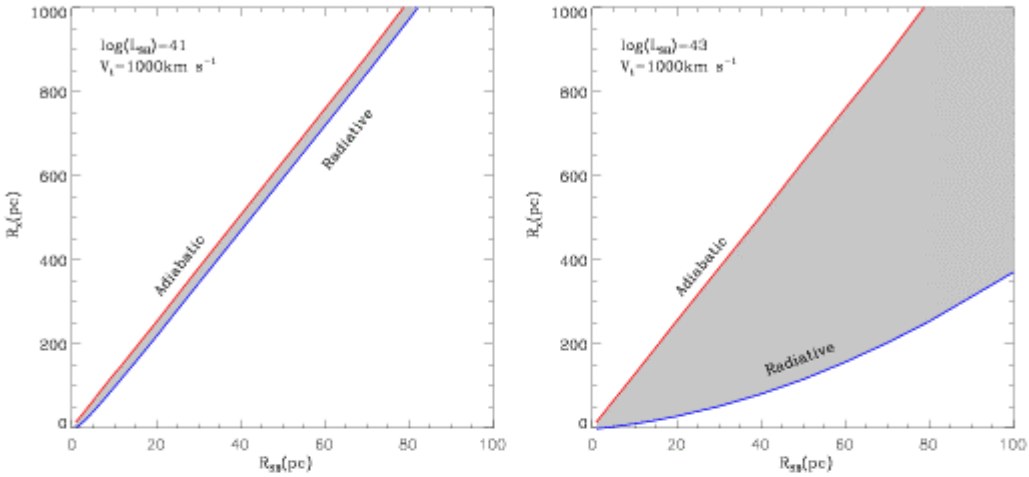


Figure 12: The X-ray zone ($T \geq 5 \times 10^5$K) cutoff radius R_x as function of R_{SB}

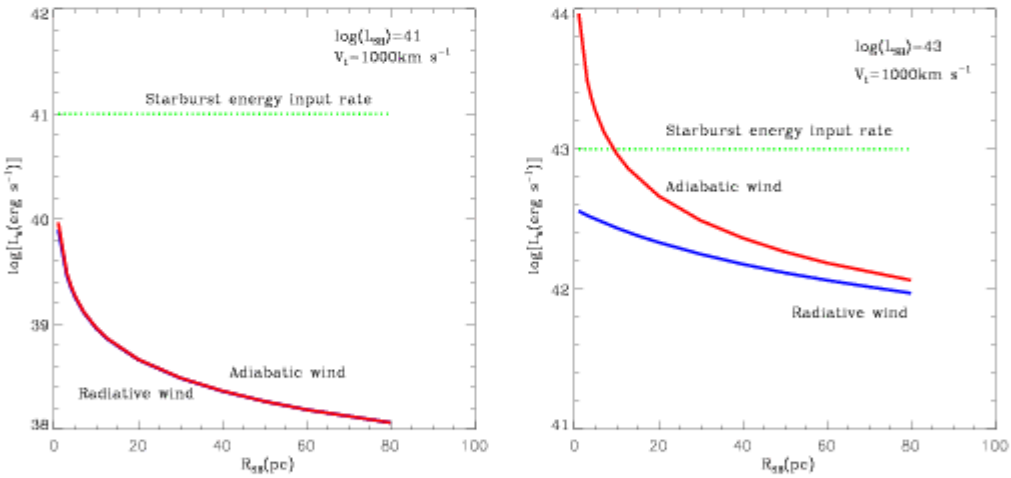


Figure 13: Superwind X-ray luminosity as function of R_{SB}

7.3 X-ray emission problems

- Low predicted luminosity
- Co-existence of the hot X-ray emitting zones and cold H_α filaments
- Low hot gas metallicity derived from the observed X-ray spectra

- **Mass loading flows ?** (Suchkov et al. 1996; Hartquist et al. 1997)
- **Thermal conductivity ?** (D'Ercole & Brighenti, 1999)
- **Non-equilibrium ionization ?** (Breitschwerdt et al. 199)
- **Well-collimated flows ?**

8 CONCLUSIONS

- Metal ejection is highly dependent on the host galaxy rotation and mass distribution. Fast rotating or stellar disk dominated galaxies are likely to undergo the phenomenon of blow-out and metal ejection into the IGM. Slow rotating systems with low mass disks and extended gaseous halos are able to prevent metal ejection into the intergalactic space unless a much larger mechanical energy is deposited.

- The comparison of the hydrodynamical models with the sample of dwarf star-forming galaxies places the bulk of the galaxy sample above the limit established for flat disk models. Indisputable contamination of their ISM by products of massive star evolution indicates that either galaxy chemical evolution is dominated by a continuous low intensity mode of star formation or metal ejection is prevented by low density gaseous halos.

- Superbubble metallicities vary with time and can easily exceed the solar value even if the host galaxy ISM has a low metal abundance. The effects of metal ejection are most noticeable during the first 10 Myr of a starburst evolution.

- Galactic superwinds driven by compact and powerful starbursts undergo catastrophic cooling close to the star cluster surface and establish temperature distributions which are radically different from the adiabatic temperature profiles.
- Dramatic fall of superwind temperature leads to shortening of the hot zone that emits X-ray radiation and decreasing of the wind X-ray luminosity.
- At the same time, cooling brings the 10^4K boundary closer to the wind center, and promotes the establishment of an extended ionized fast moving envelope. This should be detected as a week and broad (~ 1000 km s^{-1}) emission line component at the base of the much narrower line caused by the central HII region.
- The free wind model is unable to reproduce the observed superwind X-ray luminosities.